JPE 16-5-24

http://dx.doi.org/10.6113/JPE.2016.16.5.1851
ISSN(Print): 1598-2092 / ISSN(Online): 2093-4718

Ripple Analysis and Control of Electric Multiple Unit Traction Drives under a Fluctuating DC Link Voltage

Li-Jun Diao†, Kan Dong*, Shao-Bo Yin**, Jing Tang**, and Jie Chen**

†,**Department of Electronic Engineering, Beijing Jiaotong University, Beijing, China
*Locomotive and Car Research Institute, China Academy of Railway Science, Beijing, China

Abstract

The traction motors in electric multiple unit (EMU) trains are powered by AC-DC-AC converters, and the DC link voltage is generated by single phase PWM converters, with a fluctuation component under twice the frequency of the input catenary AC grid, which causes fluctuations in the motor torque and current. Traditionally, heavy and low-efficiency hardware LC resonant filters parallel in the DC side are adopted to reduce the ripple effect. In this paper, an analytical model of the ripple phenomenon is derived and analyzed in the frequency domain, and a ripple control scheme compensating the slip frequency of rotor vector control systems without a hardware filter is applied to reduce the torque and current ripple amplitude. Then a relatively simple discretization method is chosen to discretize the algorithm with a high discrete accuracy. Simulation and experimental results validate the proposed ripple control strategy.

Key words: Control algorithm discretization, Fluctuating DC link, Ripple control, Traction drives, Vector control

I. INTRODUCTION

Rail transport plays an important role in the transportation industry. In the AC-DC-AC traction systems of the EMU, the introduction of a single phase PWM converter makes the DC link contain a ripple component with twice the frequency of the line voltage. This ripple component brings about a series of harmonics in the output of an inverter, causing fluctuations in the current and torque, which causes additional harmonic heating in motors, and affects the stability and comfort of systems [1].

A hardware filter with a parallel LC resonant filter in the DC link is a traditional way to eliminate ripple voltage. However, for a high DC voltage and a low resonant frequency, it reduces the power density and increases cost due to its relatively large volume and weight. The authors of [2] simply increased the DC link capacitance to inhibit the ripple phenomenon. Although the bulky resonant inductor is removed, a capacitor with a high capacitance causes additional safety concerns. To remove bulky hardware filters, scholars have turned their research emphasis to software methods. These methods mainly include feed-forward compensation, feedback compensation, and motor frequency compensation.

Feed-forward compensation is also called pulse width compensation, where the voltage command is achieved by a motor control algorithm, and the modulation index is calculated through the instantaneous DC link voltage. Then the pulse width is reduced when the ripple voltage is positive, and vice versa. In the case of the existence of ripple DC voltage, the required motor voltage is accurately modulated [3]. The method is simple and easy to realize. However, the following problems exist: (1) accurate real-time acquisition of the DC voltage and (2) a voltage gain limit. When the ripple DC voltage is negative, it is necessary to increase the depth of the modulation. If the modulation index is high, the margin of the adjustable range is small, and the adjustable range is related to the amplitude of the ripple DC voltage. For a specific amplitude of ripple DC voltage, the adjusted modulation depth has an upper limit [4]. The effect of the feedback compensation depends on the closed-loop bandwidth. Instantaneous current feedback was proposed to suppress the ripple current, where the closed-loop output is used to correct the modulation depth by using the feedback current of the motor and the instruction current [5]. However, in the application of high power and a low switching

Manuscript received Mar. 19, 2016; accepted Jun. 10, 2016
Recommended for publication by Associate Editor Bon-Gwan Gu.
†Corresponding Author: ljdiao@bjtu.edu.cn
Tel: +86-10-51687082, Beijing Jiaotong University
*Locomotive and Car Research Institute, China Academy of Railway Science, China
**Dep. of Electronic Engineering, Beijing Jiaotong University, China

© 2016 KIPE

frequency, the bandwidth of the current loop is limited.

These three methods are rarely used because of their limited application, low precision and complex implementation. The current mainstream is frequency compensation, which uses a certain algorithm to compensate the frequency command of the motor to eliminate the ripple phenomenon. In addition, the performance of a controller in digital systems depends on the discretization method. However, none of the above references has given a discrete analysis of the proposed control strategy. Traditional digital control systems often adopt a simple and stable backward Euler discrete method, as in [6]. Unfortunately, this method cannot guarantee that the frequency characteristic of the controller remains unchanged, so it is not suitable for high precision applications. The authors of [7] describe several common discretization methods with differences in terms of accuracy, stability and complexity of digital realization. For a given controller, it is necessary to evaluate different discretization methods from the above three aspects to select an optimal one.

In this paper, a mathematical model of the traction system is established first, the transfer functions of the ripple torque and current are quantitatively derived and analyzed in the frequency domain. Then a ripple control strategy is proposed for the rotor vector control system. Finally, the algorithm is discretized by eight different methods, and the optimal discretization method for the controller is obtained after a thorough comparison of the discrete accuracy, control performance and complexity of the different digital implementations. The feasibility and effectiveness of the method will also be verified through a theoretical analysis, simulations and experiments.

II. Ripple Phenomenon Analysis in the Frequency Domain

A. Ripple Component Analysis of Traction Motors

For single phase PWM converter in traction drive systems, define U_s and I_s as the rms values of the input voltage and current, ω_{grid} as the angular frequency of the contact line, θ as the power factor angle, C_{dc} as the DC link capacitor, U_{dc} and I_{dc} as the average dc voltage and current, and $\tilde{u}_{dc}$ as the ripple component of the dc voltage, where ~ indicates the ripple components. In addition, define the input voltage and current as:

$$\begin{cases} u_s = \sqrt{2}U_s \cos(\omega_{grid} t) \\ i_s = \sqrt{2}I_s \cos(\omega_{grid} t + \theta) \end{cases} \tag{1}$$

Then the instantaneous input ac power and the output dc power can be written as:

$$\begin{cases} P_i = u_s i_s = U_s I_s \cos\theta + U_s I_s \cos(2\omega_{grid} t + \theta) \\ P_o = U_{dc} I_{dc} + C_{dc} U_{dc} \dfrac{d\tilde{u}_{dc}}{dt} \end{cases} \tag{2}$$

Both powers consist of a stable part and a ripple part. Omitting the loss of the PWM converter, the two parts of the input and output powers can be assumed to be equal. Then the following is obtained:

$$\tilde{u}_{dc} = \frac{I_{dc} \sin(2\omega_{grid} t + \theta)}{2\omega_{grid} C_{dc} \cos\theta} \tag{3}$$

The ripple frequency is twice the grid frequency, and the amplitude is related to the traction power, the DC link capacitor and the single phase converter's power factor. When the traction inverter operates at twice the grid frequency, the ripple phenomenon is very serious.

To further analyze the nature of the ripple phenomenon, a mathematical model of the traction system has to be derived. The following equation can be derived from the derivation of the voltage and flux functions under rotating coordinate [8]:

$$\begin{bmatrix} V_{sd} \\ V_{sq} \\ 0 \\ 0 \end{bmatrix} = \begin{bmatrix} R_s + sL_s & -\omega_e L_s & sL_m & -\omega_e L_m \\ \omega_e L_s & R_S + sL_s & \omega_e L_m & sL_m \\ sL_m & -\omega_{sl} L_m & R_r + sL_r & -\omega_{sl} L_r \\ \omega_{sl} L_m & sL_m & \omega_{sl} L_r & R_r + sL_r \end{bmatrix} \begin{bmatrix} I_{sd} \\ I_{sq} \\ I_{rd} \\ I_{rq} \end{bmatrix} \tag{4}$$

where R_s and R_r are the stator and rotor resistances, L_s and L_r are the stator and rotor inductances, L_m is the magnetizing inductance, ω_e is the stator angular frequency, ω_{sl} is the slip angular frequency, I_{sd} and I_{sq} are the d-axis and q-axis currents of the stator, I_{rd} and I_{rq} are the d-axis and q-axis currents of the rotor, and s is the Laplace operator.

Split the coefficient matrix of (4) into a derivative part and a non-derivative part. After simplifying, the following is obtained:

$$s \begin{bmatrix} I_{sd} \\ I_{sq} \\ I_{rd} \\ I_{rq} \end{bmatrix} = A \begin{bmatrix} I_{sd} \\ I_{sq} \\ I_{rd} \\ I_{rq} \end{bmatrix} + D \begin{bmatrix} V_{sd} \\ V_{sq} \end{bmatrix} \tag{5}$$

where:

$$A = \begin{bmatrix} -\dfrac{R_s}{L_s\sigma} & \dfrac{\omega_r}{\sigma} + \omega_{sl} & \dfrac{R_r L_m}{L_r L_s \sigma} & \dfrac{L_m \omega_r}{L_s \sigma} \\ -\dfrac{\omega_r}{\sigma} - \omega_{sl} & -\dfrac{R_s}{L_s\sigma} & -\dfrac{L_m \omega_r}{L_s \sigma} & \dfrac{R_r L_m}{L_r L_s \sigma} \\ \dfrac{L_m R_s}{L_r L_s \sigma} & -\dfrac{L_m \omega_r}{L_r \sigma} & -\dfrac{R_r}{L_r \sigma} & -\dfrac{L_m^2 \omega_r}{L_r L_s \sigma} + \omega_{sl} \\ \dfrac{L_m \omega_r}{L_r \sigma} & \dfrac{L_m R_s}{L_r L_s \sigma} & \dfrac{L_m^2 \omega_r}{L_r L_s \sigma} - \omega_{sl} & -\dfrac{R_r}{L_r \sigma} \end{bmatrix}$$

$$D = \begin{bmatrix} \dfrac{1}{L_s\sigma} & 0 \\ 0 & \dfrac{1}{L_s\sigma} \\ -\dfrac{L_m}{L_r L_s \sigma} & 0 \\ 0 & -\dfrac{L_m}{L_r L_s \sigma} \end{bmatrix}, \quad \sigma = 1 - \frac{L_m^2}{L_r L_s}$$

For further analysis, write (5) in the form of steady-state components (with the subscript 0) and small fluctuation components:

$$s(I_0+\tilde{I})=(A_0+\tilde{A})(I_0+\tilde{I})+D(V_0+\tilde{V}) \tag{6}$$

From (6) it is possible to obtain the relationships among the respective ripple components:

$$s\tilde{I}=A_0\tilde{I}+\tilde{A}I_0+D\tilde{V} \tag{7}$$

This can be further simplified as:

$$Z(s)\begin{bmatrix}\tilde{I}_{sd}\\ \tilde{I}_{sq}\\ \tilde{I}_{rd}\\ \tilde{I}_{rq}\end{bmatrix}=G\begin{bmatrix}\tilde{V}_{sd}\\ \tilde{V}_{sq}\\ \tilde{\omega}_r\\ \tilde{\omega}_{sl}\end{bmatrix} \tag{8}$$

where:

$$Z(s)=sI-A_0$$

$$G=\begin{bmatrix}\frac{1}{L_s\sigma} & 0 & \frac{L_sI_{sq0}+L_mI_{rq0}}{L_s\sigma} & I_{sq0}\\ 0 & \frac{1}{L_s\sigma} & -\frac{L_sI_{sd0}+L_mI_{rd0}}{L_s\sigma} & -I_{sd0}\\ -\frac{L_m}{L_rL_s\sigma} & 0 & -\frac{L_mL_sI_{sq0}+L_m^2I_{rq0}}{L_rL_s\sigma} & I_{rq0}\\ 0 & -\frac{L_m}{L_rL_s\sigma} & \frac{L_sL_mI_{sd0}+L_m^2I_{rd0}}{L_rL_s\sigma} & -I_{rd0}\end{bmatrix}$$

Then the relationship among the ripple currents, the ripple voltage under d-q axis, and slip frequency of the traction motor can be derived as:

$$\begin{bmatrix}\tilde{I}_{sd}\\ \tilde{I}_{sq}\\ \tilde{I}_{rd}\\ \tilde{I}_{rq}\end{bmatrix}=\left[Z(s)\right]^{-1}D\begin{bmatrix}\tilde{V}_{sd}\\ \tilde{V}_{sq}\end{bmatrix}=2\pi\left[Z(s)\right]^{-1}\begin{bmatrix}I_{sq0}\\ -I_{sd0}\\ I_{rq0}\\ -I_{rd0}\end{bmatrix}\tilde{f}_{sl} \tag{9}$$

B. Mathematic Model of the Ripple Phenomenon

Motor torque can be expressed as [9]:

$$T_e=\frac{3}{2}pL_m(i_{sq}i_{rd}-i_{sd}i_{rq}) \tag{10}$$

where p is the number of motor pole pairs.

To simplify the analysis, approximately divide the physical items of the traction motor into two parts: the sustainable part x_0 produced by the average dc voltage and the ripple part $\tilde{x}$ produced by the ripple dc voltage, which can be written as:

$$x=x_0+\tilde{x} \tag{11}$$

Then the ripple torque of the traction motor can be derived as:

$$\tilde{T}_e=T_e-T_{e0}=\frac{3pL_m}{2}\left[\left(i_{sq}i_{rd}-i_{sd}i_{rq}\right)-\left(i_{sq0}i_{rd0}-i_{sd0}i_{rq0}\right)\right] \tag{12}$$

Substitute (11) into (12), simplify it and omit the multiplied ripple parts. (12) can then be written in the form of matrix multiplication as (13). Then define the d and q parts of the stator voltage V_s as $\begin{bmatrix}V_{sd}\\ V_{sq}\end{bmatrix}=V_s\begin{bmatrix}\cos\phi\\ \sin\phi\end{bmatrix}$, and the modulation index as $m=\pi V_s/(2u_{dc})$. Combining (6) and (13), it is possible to obtain the ripple torque transfer function as (14).

TABLE I
MAIN PARAMETERS OF TRACTION INDUCTION MOTOR

V_N	rated stator line voltage	1287 V
I_N	rated stator current	88 A
P_N	rated power	160 kW
f_N	rated stator frequency	84 Hz
R_s	stator resistance	0.223Ω
R_r	rotor resistance	0.103Ω
L_m	magnetic inductance	0.0438 H
L_s	stator inductance	0.04538 H
L_r	rotor inductance	0.045876 H
p	pole pair	2

$$\tilde{T}_e=\frac{3pL_m}{2}\begin{bmatrix}-i_{rq0}\\ i_{rd0}\\ i_{sq0}\\ -i_{sd0}\end{bmatrix}^{\mathrm{T}}\begin{bmatrix}\tilde{I}_{sd}\\ \tilde{I}_{sq}\\ \tilde{I}_{rd}\\ \tilde{I}_{rq}\end{bmatrix} \tag{13}$$

$$G_{T_eu}(s)=\frac{\tilde{T}_e}{\tilde{u}_{dc}}=\frac{3m}{\pi}pL_m\begin{bmatrix}-i_{rq0}\\ i_{rd0}\\ i_{sq0}\\ -i_{sd0}\end{bmatrix}^{\mathrm{T}}\left[Z(s)\right]^{-1}D\begin{bmatrix}\cos\phi\\ \sin\phi\end{bmatrix} \tag{14}$$

It is possible to derive the ripple current transfer function in the same way. Describe the stator current and its d and q axis components by (11) and square them. Then the following is obtained:

$$I^2=I_0^2+\tilde{I}^2+2I_0\tilde{I} \tag{15}$$

$$I_{sd}{}^2=I_{sd0}^2+\tilde{I}_{sd}^2+2I_{sd0}\tilde{I}_{sd} \tag{16}$$

$$I_{sq}{}^2=I_{sq0}^2+\tilde{I}_{sq}^2+2I_{sq0}\tilde{I}_{sq} \tag{17}$$

Combine the three equations and ignore the square values of the ripple components, then:

$$\tilde{I}=\frac{1}{I_0}\begin{bmatrix}I_{sd0}\\ I_{sq0}\end{bmatrix}^{\mathrm{T}}\begin{bmatrix}\tilde{I}_{sd}\\ \tilde{I}_{sq}\end{bmatrix} \tag{18}$$

Combining with (6), the ripple current transfer function can be written as:

$$G_{Iu}(s)=\frac{\tilde{I}}{\tilde{u}_{dc}}=\frac{2m}{\pi I_0}\begin{bmatrix}I_{sd0}\\ I_{sq0}\end{bmatrix}^{\mathrm{T}}\left[Z(s)\right]_{2\times4}^{-1}D\begin{bmatrix}\cos\phi\\ \sin\phi\end{bmatrix} \tag{19}$$

C. Frequency Domain Analysis

To analyze the model, an actual traction motor is taken as an example. The motor parameters are listed in Table I.

The simulation was taken under the condition m=1. Fig. 1 and Fig. 2 give the ripple torque and current characteristics in the frequency domain. It can be seen that the amplitude of the ripple torque and current both reach the maximum value when the motor is operating at a ripple frequency of 100Hz.

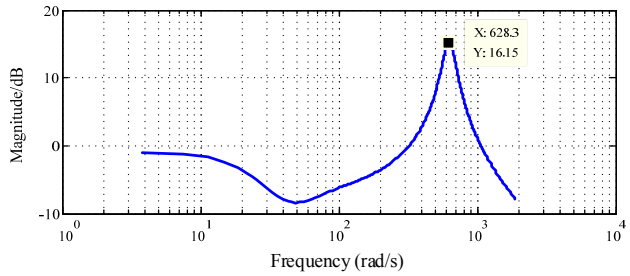

Fig. 1. Frequency characteristics of ripple torque.

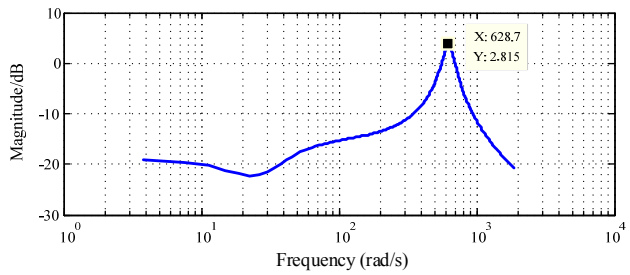

Fig. 2. Frequency characteristics of ripple current.

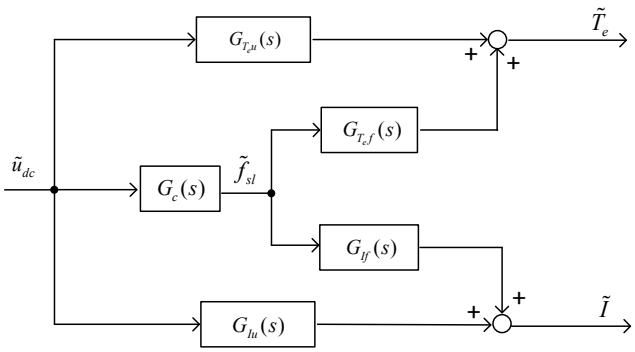

Fig. 3. The proposed ripple control scheme.

III. Ripple Controller Design Based on Frequency Domain Analysis

Substituting (6) into (13) and (18), it is possible to obtain the transfer functions between the ripple torque, ripple current and slip frequency increment as:

$$G_{T_e f}(s)=\frac{\tilde{T}_e}{\tilde{f}_{sl}}=3\pi pL_m\begin{bmatrix}-i_{rq0}\\ i_{rd0}\\ i_{sq0}\\ -i_{sd0}\end{bmatrix}^{\mathrm{T}}[Z(s)]^{-1}\begin{bmatrix}I_{sq0}\\ -I_{sd0}\\ I_{rq0}\\ -I_{rd0}\end{bmatrix} \tag{20}$$

$$G_{If}(s)=\frac{\tilde{I}}{\tilde{f}_{sl}}=\frac{2\pi}{I_0}\begin{bmatrix}I_{sd0}\\ I_{sq0}\end{bmatrix}^{\mathrm{T}}[Z(s)]^{-1}_{2\times 4}\begin{bmatrix}I_{sq0}\\ -I_{sd0}\\ I_{rq0}\\ -I_{rd0}\end{bmatrix} \tag{21}$$

Using the ripple component of the dc voltage as an input, define the ripple controller $G_c(s)$ as shown in Fig. 3 to modify the slip frequency of the traction motor.

From the above analysis it is known that the ripple phenomenon is at its most serious at the ripple frequency ω_{ripple}. To make the ripple torque and current as small as possible, the ripple controller is proposed as:

$$G_c(s)=K\frac{s\omega_{ripple}}{(s+\omega_{ripple})^2} \tag{22}$$

where, K is the compensation coefficient.

An ideal value of K should make the amplitude of the ripple torque and current both at their minimum. However, it is hard to find a value to satisfy both conditions at the same time. An analysis of the ripple torque and current is made to get the optimal K value.

From (14), (20) and (22), the amplitude of the ripple torque is related to the compensation coefficient K, the angle between the voltage vector and the d axis Φ, and the modulation index m. It is clear that the amplitude increases with m. In order to explore this influence, the modulation index is fixed as 1, and the motor parameters are used as shown in Table I to calculate the amplitude of the ripple torque. The result is shown in Fig. 4, where the x-axis stands for the voltage angle, the y-axis stands for the compensation coefficient, and the z-axis stands for the amplitude of the ripple torque.

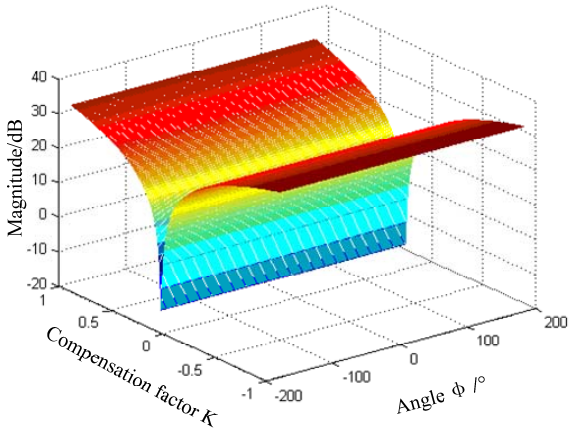

Fig. 4. Ripple torque amplitude versus compensation coefficient and voltage angle.

From Fig. 4 it can be seen that the ripple torque has nothing to do with Φ, and the relationship with K is a curve, where the ripple torque amplitude increases with a large absolute K. It reaches its minimum value at the point (0.136,-14.4dB), i.e. the compensation performance of the ripple torque is the best when K is 0.136. In the same way, it is possible to obtain the characteristics of the ripple current amplitude, which looks quite similar to Fig. 4, where the ripple current has nothing to do with Φ, and K = 0.132 is the best choice.

By balancing the compensation performance of the torque and current, the optimal compensation coefficient becomes K = 0.134. Fig. 5 and Fig. 6 show amplitude-frequency characteristic curves of the ripple torque and current under this coefficient. Compared with Fig. 1 and Fig. 2, after compensation, the ripple torque amplitude decreased from

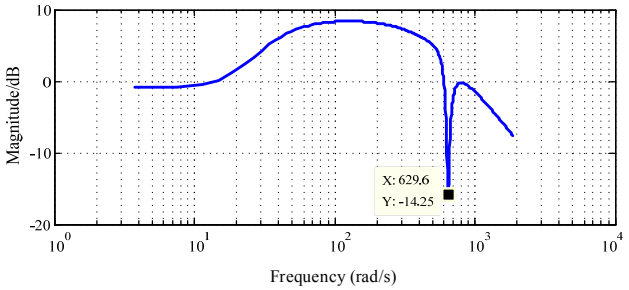

Fig. 5. Amplitude characteristics of ripple torque after compensation.

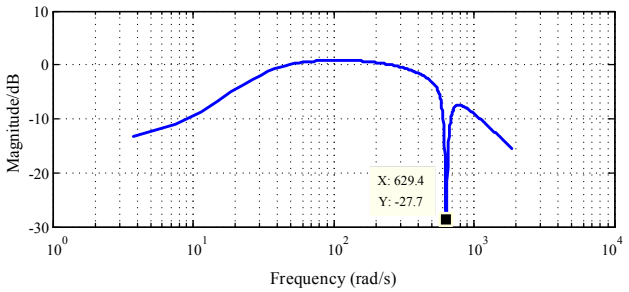

Fig. 6. Amplitude characteristics of ripple current after compensation.

15dB to -33dB, and the ripple current amplitude decreased from the original 2.4dB to -61dB. The compensation effect is obvious.

IV. Discretization of the Ripple Controller

The digital control performance depends on the discretization method. At present, the general discretization methods are divided into five categories, as described in [10] and [11]: (1) the Euler method, including the Forward Euler (FWE) and the Backward Euler (BWE); (2) the Hold method, including the Zero-Order Hold (ZOH) and the First-Order Hold (FOH); (3) the Bilinear method, including the Tustin Transformation (TUS) and the bilinear transformation with pre-warping (PRE); (4) the Impulse invariant method (IMP); and (5) Zero-Pole Matching (ZPM). Using these methods, (22) can be discretized according to [11]. The results are shown in Table II.

In this table, the coefficients are shown as follows:

$A = K\omega_{ripple}T_s$, $B = \omega_{ripple}T_s$, $C = K\omega_{ripple}$.

$a_0 = -Be^{-2B}$, $a_1 = 2Be^{-B} + Be^{-2B}$, $a_2 = -B - 2Be^{-B}$.

$b_0 = (A-K)e^{-B} + Ke^{-2B}$,

$b_1 = K + (K-3A)e^{-B} - 2Ke^{-2B}$,

$b_2 = -2K + (K+3A)e^{-B} + Ke^{-2B}$,

$b_3 = K - (K+A)e^{-B}$.

$m = K\omega_{ripple}^2 \tan(\frac{\omega_{ripple}T_s}{2})$,

$n_0 = \omega_{ripple}^2 (1-\tan(\frac{\omega_{ripple}T_s}{2}))^2$,

TABLE II
Discrete Expression of Gc(s)

FWE	$\frac{Az-A}{z^2-2(1-B)z+(1-B)^2}$
BWE	$\frac{Az^2-Az}{(1+B)^2z^2-2(1+B)z+1}$
ZOH	$\frac{Ae^{-B}z-Ae^{-B}}{z^2-2e^{-B}z+e^{-2B}}$
FOH	$\frac{b_3z^3+b_2z^2+b_1z+b_0}{Bz^3+a_2z^2+a_1z+a_0}$
TUS	$\frac{2Az^2-2A}{(2+B)^2z^2+2(B^2-4)z+(2-B)^2}$
ZPM	$\frac{T_sC(z-1)}{z^2-2e^{-B}z+e^{-2B}}$
IMP	$\frac{T_s(Cz^2-(C+A\omega_{ripple})e^{-B}z)}{z^2-2e^{-B}z+e^{-2B}}$
PRE	$\frac{m(z^2-1)}{n_2z^2-n_1z+n_0}$

$n_1 = 2\omega_{ripple}^2(1-\tan^2(\frac{\omega_{ripple}T_s}{2}))$,

$n_2 = \omega_{ripple}^2(1+\tan(\frac{\omega_{ripple}T_s}{2}))^2$.

From Table II, the methods of the ZOH, FOH, ZPM, IMP, and PRE all introduce nonlinear factors, which make their implementation complicated, whereas the implementations of the FWE, BWE and TUS are relatively simple.

Fig. 7 gives the amplitude-frequency characteristics of the FWE and BWE and continuous function under an iterative calculation frequency of 1 kHz. From the results, it can be seen that the characteristics have changed after the FWE and BWE transformations: the amplitude of the continuous function is -23.61 dB at a ripple frequency of 100Hz, whereas after the FWE and BWE transformations, the amplitudes are -22.14 dB and -24.84 dB, respectively.

Fig. 8 shows the amplitude-frequency characteristics of the ZOH, FOH, PRE, TUS, ZPM, IMP and continuous function. It can be seen that all of the discrete methods have good performance within a given frequency range. Whereas, from the enlarged view near the ripple frequency, it can be seen that the different methods have small differences. The TUS and PRE methods are the most similar to the continuous function.

From Fig. 7 and Fig. 8, it can be seen that although the FWE and BWE are simple to realize, there is an amplitude attenuation at the ripple frequency; the IMP method guarantees the consistency of the impulse response, but in the whole speed range, there is a significant deviation amplitude; the amplitude-frequency characteristics of the ZOH, FOH, ZPM, TUS and PRE are quite consistent with those of the continual method, but from an enlarged view near the ripple frequency, it can be seen, that the TUS and PRE are better than the other methods. Based on the above analysis, the TUS is chosen as the discretization method for the ripple

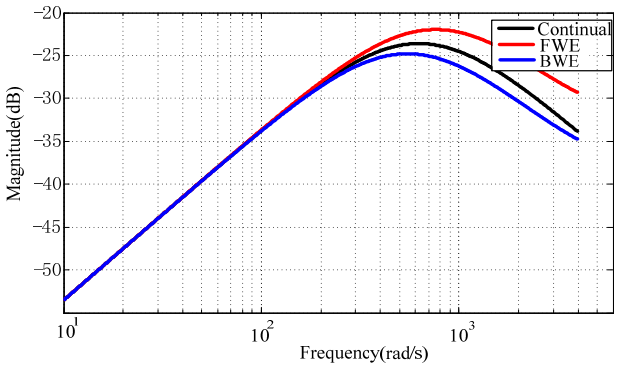

Fig. 7. Amplitude-frequency characteristics of FWE, BWE and continuous function.

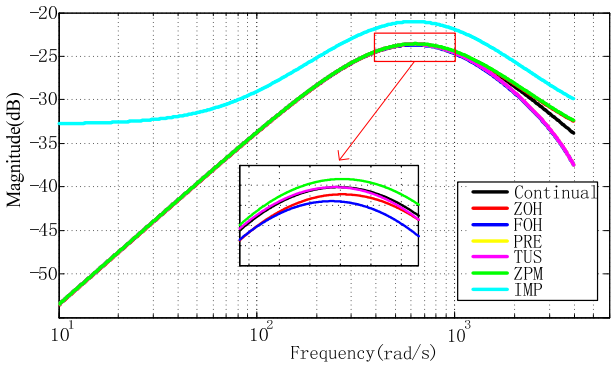

Fig. 8. Amplitude-frequency characteristics of ZOH, FOH, PRE, TUS, ZPM, IMP and continuous function.

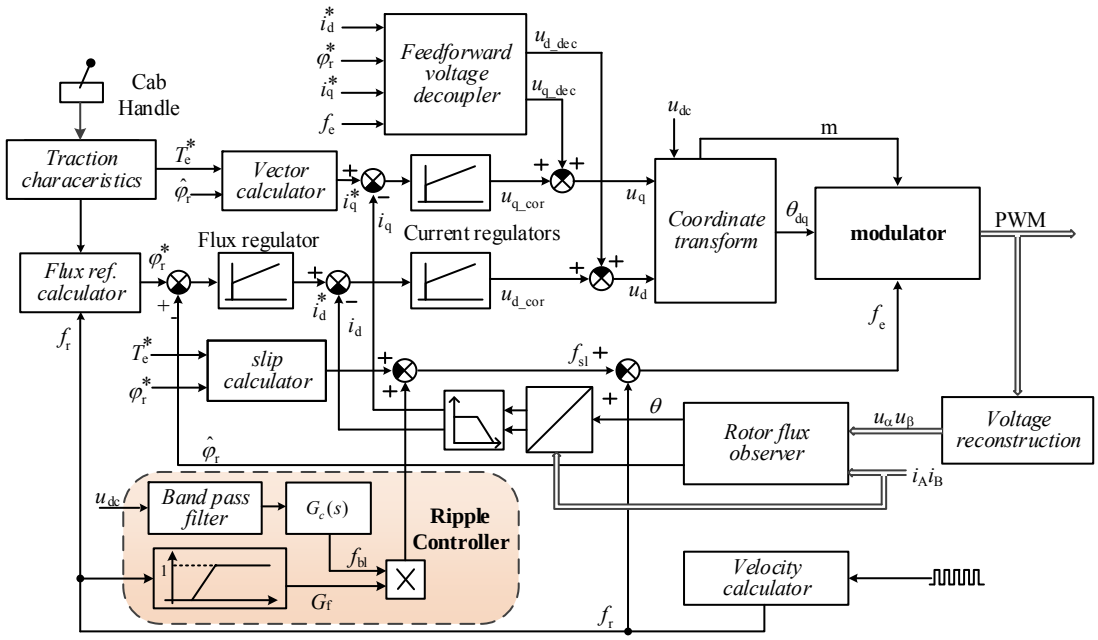

Fig. 9. Schematic of vector control with demonstrated ripple controller.

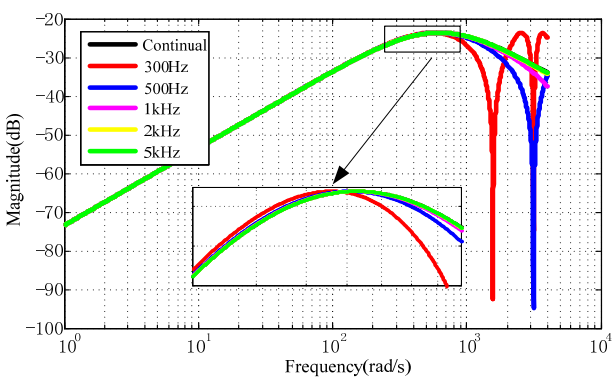

Fig. 10. Discrete accuracy of TUS with different iterative frequencies.

controller, since the TUS method has a higher discrete accuracy and is easier to implement.

Fig. 10 gives the amplitude-frequency characteristics of the TUS under different iterative calculation frequencies. It shows that the discretization errors decrease gradually with an increasing iterative frequency. In EMU applications, the maximum stator frequencies of traction motors are often between 120 and 250Hz, i.e. between 750rad/s and 1600rad/s. From the curves, it can be seen that the discrete errors under iterative frequencies with 300Hz and 500Hz are too high to meet the requirements of the controller. However, it can ensure higher discrete accuracy when the iterative frequencies are 1kHz, 2kHz and 5kHz. Considering the algorithm load of the control unit, an iterative frequency of 1kHz is chosen.

V. Simulation and Experiment Validation

A. Simulation Analysis

To verify the ripple control method, a simulation model has been built in the Matlab/Simulink environment, where the power supply is 900Vac/50Hz, the rated DC link voltage is 1650V with a 8mF DC link capacitor, the LC resonant filter is consisted of a 0.362mH inductance and a 7mF capacitor.

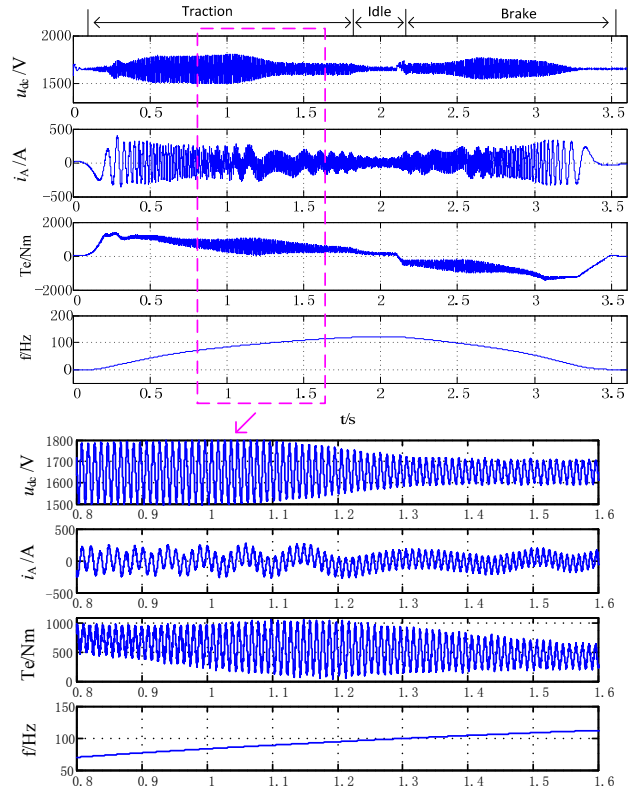

Fig. 11. Ripple phenomenon simulation without LC filter.

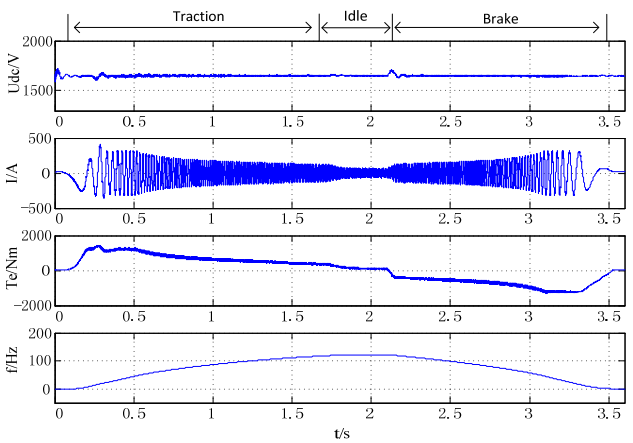

Fig. 12. Simulation results with LC filter.

The maximum switching frequency of the inverter is 1kHz, the rated power of the traction motor is 160kW, the rated frequency is 84Hz, and the other motor parameters are shown in Table I.

Fig. 9 gives a vector control schematic for the traction motor, and in the FOC strategy, the basic slip frequency is calculated directly by the reference torque and flux. The given ripple control algorithm is inside the dotted line. The band pass filter is used to extract the DC voltage ripple component. After the amplitude-phase compensation, the ripple controller uses the ripple component to calculate the frequency offset f_{bl}. In fact, the ripple phenomenon effect is not quite obvious at low frequencies, such as a frequency lower than 20Hz.

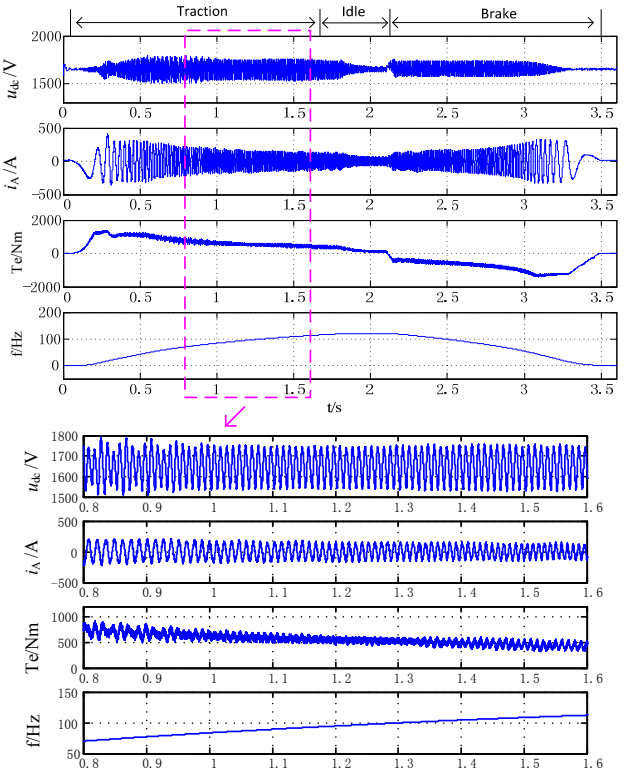

Fig. 13. Simulation results of ripple control strategy without LC filter.

Therefore, an additional high pass filter is needed to remove the low frequency effect by multiplying the gain factor G_f with f_{bl}. G_f will only be active when the motor reaches to a frequency higher than 20Hz. Then the final frequency offset is added to the output frequency of the FOC to suppress the ripple phenomenon.

For all of the simulations, the motor accelerates from a standstill to 120Hz by the maximum traction torque. Then it idles without torque. At 2.1s, the motor brakes by the maximum braking torque to stop. Fig. 11 shows simulation results of the ripple phenomenon after removing the DC link LC resonant filter. It can be seen that the amplitude of the DC voltage ripple component is proportional to the inverter power. This is consistent with (3). The amplitude of the ripple current and torque near the ripple frequency (100Hz) are much more serious than those in other frequency ranges, as can be seen in the enlarged figure at the bottom of Fig. 11. The simulation results of the system with a parallel LC resonant filter are given in Fig. 12, where no twice frequency exit in the DC voltage, and the traction performance is normal. The simulation results of the ripple control strategy can be seen in Fig. 13. It is obvious that the ripple current and torque of the motor have been significantly suppressed. The performance near a ripple frequency of 100Hz can also be seen in the enlarged part at the bottom. The simulation results of the three cases verify that the proposed strategy has a good suppression effect on the ripple components, and that the

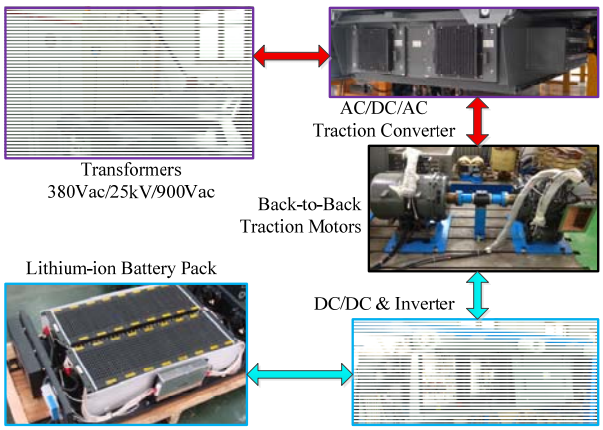

Fig. 14. Sketch map of the test platform for ripple control.

hardware LC resonance filter can be cancelled.

B. Experimental Verification

To further verify the proposed control strategy, a DSP and a field programmable gate array (FPGA) are used to do the programming, and virtual instrument means are used for the purpose of sending instructions, status monitoring and waveform recordings through the Ethernet. Considering that the amplitude of the DC ripple voltage is proportional to its load, in order to simulate the actual ripple phenomenon of a train as far as possible, the power rate of the test system cannot be too small. At the same time, the power available in the lab is limited, so 100kW is chosen as the load power rate, and the DC link capacitance is reduced by 50%. The experimental platform shown in Fig. 14 is adopted, the AC-DC-AC traction converter (which employs the two-level IGBT topology and is used for actual EMU trains) under testing is power by a 25kV/900Vac traction transformer, where a 380Vac/25kV single phase high voltage transformer is used to connect to the lab ac grid. Instead of using the traditional common DC side of the mutual power feed mode, an additional lithium-ion battery package controlled by a bidirectional DC-DC converter is used to power the test motor-inverter system.

Then three sets of experiments are designed, including a DC side without a LC resonant filter and no compensation control, a DC side parallel hardware resonant filter, and no resonant filter but using a ripple control strategy. In all of the tests, the motor is accelerated to the ripple frequency (100Hz) and maintained at a constant speed. The waveforms of the DC voltage, motor current, ripple DC component and motor speed are obtained by a virtual oscilloscope based on Ethernet with a 10 kHz sampling frequency.

Fig. 15 gives the waveforms without a LC filter or a ripple control strategy. The amplitude of the ripple DC voltage is about 25V, and there is an obvious low frequency fluctuation of the motor current. In addition, the ripple current amplitude is about 30A, which is basically consistent with the theoretical results from (19) and Fig. 2, where:

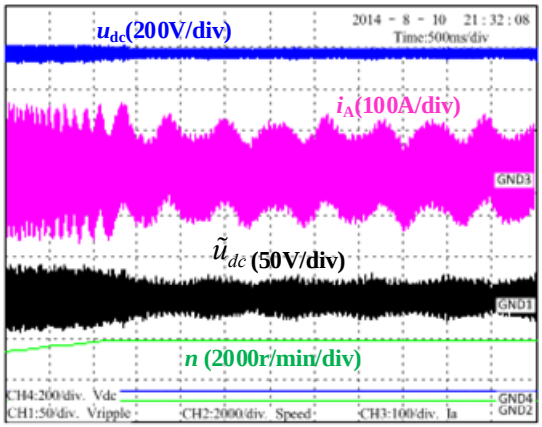

Fig. 15. Experiment results without ripple control and resonant filter.

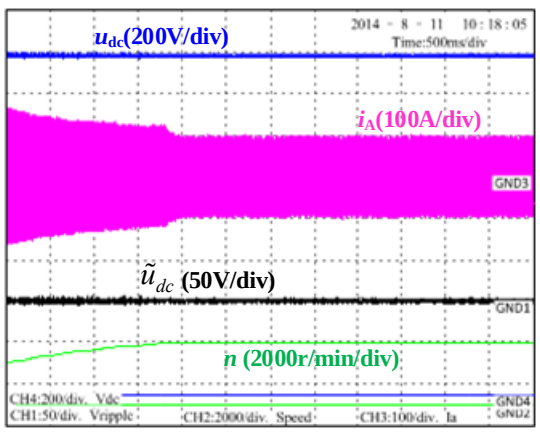

Fig. 16. Experiment results with hardware LC filter.

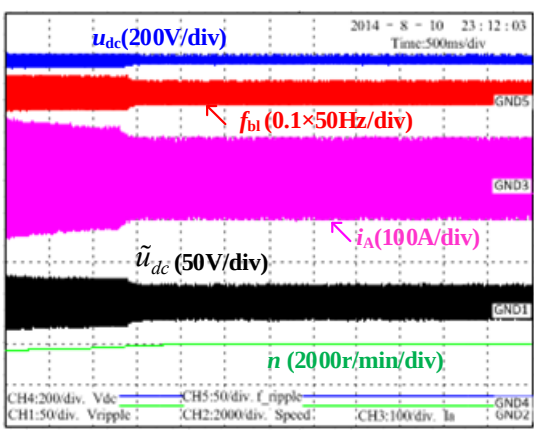

Fig. 17. Experiment results under ripple control.

$$\left|\tilde{I}\right| = \left|G_{Iu}(j\omega_{ripple})\right|_{m=1} \tilde{u}_{dc} = 10^{2.815/20} \times 25 \approx 34.57 \text{ A}.$$

Fig. 16 shows the results for a system with a LC resonant filter. The DC voltage has almost no ripple component, and the motor current is relatively stable.

Fig. 17 shows the results under ripple control, where the compensation frequency f_{bl} varies with the DC voltage ripple component. It can be seen that with the ripple control algorithm, the low frequency ripple of the motor current is

suppressed, which is similar to the simulation results. It can also be seen that the ripple DC voltage becomes more stable compared to Fig. 15. This shows that the suppressed ripple motor current after the implementation of the ripple control is helpful for DC voltage stability.

VI. Conclusion

In the electric traction systems of an EMU, because of the single phase PWM converter, there is ripple component in the DC link with twice the basic frequency of the ac grid. This ripple phenomenon causes ripple torque and current. In this paper, the ripple phenomenon is analyzed in the frequency domain. Then a ripple control scheme is proposed for the rotor vector control system. The implementation of this algorithm and the parameter design in a digital system is also studied in detail. The ripple controller is discretized with eight methods to choose the optimal discretization method, by comparisons of the discrete precision, control performance and implementation complexity. The algorithm is verified by simulations and experimental results, where the ripple phenomenon is suppressed according to the calculations.

Acknowledgment

This work was supported by the China National Science and Technology Support Program under Grant 2013BAG21QB00, the China National Natural Science Foundation under Grant U1134204 and the Fundamental Research Funds for the Central Universities under Grant 2016JBM058.

References

[1] J. Klima, "Analytical investigation of influence of DC link voltage ripple on PWM VSI fed induction motor drive," *Proc. of IEEE Conference on Industrial Electronics and Applications*, pp. 1-7, 2006.

[2] P. Dahler and G. Knapp, "New generation of compact low voltage IGBT converter for traction applications," *European Conference on Power Electronics and Applications*, pp. 1-9, 2005.

[3] K. Samir and L. Pablo, "Multicarrier PWM with DC link ripple feed-forward compensation for multilevel inverters," *IEEE Trans. Power Electron.*, Vol.23, No.1, pp. 52-59, Jan. 2008.

[4] P. N. Enjeti and W. Shireen, "A new technique to reject DC link voltage ripple for inverters operating on programmed PWM waveforms," *IEEE Trans. Power Electronics*, Vol.7, No.1, pp.171-180, Jan. 1992.

[5] M. E. de Oliveira Filho, J. R. Gazoli, A. J. S. Filho, and E. R. Filho "A control method for voltage source inverter without dc link capacitor," in *conf. Power Electronics Specialists*, pp. 4432-4437, 2008.

[6] B. Wang, Y. Yu, W. Sun, G. L. Wang, and D. G. Xu, "A modified discretization method for discrete full-order flux observer of induction motor," in *17th European Conf. Power Electronics and Applications (EPE'15 ECCE)*, pp. 1-6, 2015.

[7] G. F. Franklin, J. D. Powell, and M. Workman, *Digital Control of Dynamic Systems*, 3rd ed., Addison-Wesley, Chap. 6. 1997.

[8] A. Kimura, "A study on the stabilization of control systems for induction motor-driven rolling stock," *Electrical Engineering in Japan*, Vol.110, No.4, pp.101-110, 1990.

[9] B. K. Bose, *Modern Power Electronics and AC Drives*, China Machine Press, Chap. 2, 2005.

[10] F. J. Rodriguez, E. Bueno, M. Aredes, and L. G. B. Rolim, "Discrete-time implementation of second order generalized integrators for grid converters," in *34th Annu. Conf. IEEE Industrial Electronics*, pp. 76-181, 2008.

[11] A. G. Yepes, F. D. Freijedo, J. Doval-Gandoy, O. Lopez, J. Malvar, and P. Fernandez-Comesana, "Effects of discretization methods on the performance of resonant controllers," *IEEE Trans. Power Electron.*, Vol. 25, No. 7, pp. 1692-1712, Jul. 2010.

Li-Jun Diao was born in Guangdong, China, in 1980. He received his B.S. and Ph.D. degrees in Electrical Engineering from Beijing Jiaotong University, Beijing, China, in 2003 and 2008, respectively. From 2008 to 2010, he worked as a Postdoctoral Researcher of Traffic Transportation Engineering in Beijing Jiaotong University, where he was in charge of the traction system for the first 100% low-floor vehicle in China. He is presently working as an Associate Professor in the Department of Electrical Engineering, Beijing Jiaotong University. His current teaching and research interests include power electronics, variable-frequency drives, power semiconductors and their applications, and rail transportation traction control and safety.

Kan Dong was born in Shandong, China, in 1987. He received his B.S. and Ph.D. degrees in Electrical Engineering from Beijing Jiaotong University, Beijing, China, in 2010 and 2015, respectively. Since 2015, he has been an Research Assistant in the Locomotive and Car Research Institute, China Academy of Railway Sciences, Beijing, China. His current research interests include power electronics and ac drives in various industrial fields.

Shao-Bo Yin was born in Hebei, China, in 1994. He received his B.S. degree in Electrical Engineering from Beijing Jiaotong University, Beijing, China, in 2015, where he is presently working towards his Ph.D. degree. His current research interests include power electronics, power semiconductors and their applications, and rail transportation traction control.

Jing Tang was born in Hubei, China, in 1993. She received her B.S. degree in Electrical Engineering from Beijing Jiaotong University, Beijing, China, in 2014. She is presently working towards her Ph.D. degree in Power Electronics and Power Drives at Beijing Jiaotong University.

Jie Chen was born in Zhejiang, China, in 1986. He received his B.S. and Ph.D. degrees in Electrical Engineering from Beijing Jiaotong University, Beijing, China, in 2008 and 2013, respectively. Since 2013, he has been a Postdoctoral Researcher in the Institute of Electrical Engineering Chinese Academy of Sciences, Beijing, China. From 2014 to 2015, he was a Visiting Scholar at the Wisconsin Electric Machines and Power Electronics Consortium (WEMPEC), University of Madison, Madison, WI, USA. He is presently working as an Associate Professor in Beijing Jiaotong University. His current research interests include variable frequency drives, rail transportation traction control, and inverter parallel control.